Published in final edited form as:

Magn Reson Med. 2019 March ; 81(3): 1947–1954. doi:10.1002/mrm.27520.

Imaging of a high concentration of iron labeled cells with positive contrast in a rat knee.

Sergey Magnitsky[1,4,*], **Stephan Pickup**[3], **Michael Garwood**[2], and **Djaudat Idiyatullin**[2]

[1]Department of Radiology and Biomedical Imaging, University of California, San Francisco, CA, USA

[2]Center for Magnetic Resonance Research and Department of Radiology, University of Minnesota, Minneapolis, MN, USA

[3]Department of Radiology, University of Pennsylvania, Philadelphia, PA, USA

[4]current address: Children's Hospital of Philadelphia, Small Animal Imaging facility, Philadelphia PA, USA

Abstract

Purpose: The SWIFT imaging technique has been shown to provide positive contrast from diluted cell suspensions labeled with super-paramagnetic iron oxide (SPIO) in a tissue, as an alternative to T2*-weighted imaging. Here we demonstrate a variation of the SWIFT technique that yields a hyperintense signal from a concentrated cell suspension. The proposed technique provides minimal background signal from host tissue and facilitates visualization of injected cells.

Methods: The proton resonance frequency and linewidth were determined for SPIO solutions of different concentrations. The original SWIFT sequence was modified and a dual saturation Gaussian shape RF pulse with ~200 Hz bandwidth was incorporated into the acquisition protocol to suppress host tissue and fat signals. This modification of the original acquisition protocol permits the detection of a hyperintense signal from grafted cells with minimal background signal from the host tissue.

Results: SPIO particles not only induce broadening of NMR line-width but also an initiate proton resonance frequency shift. This shift is linearly proportional to the concentration of the iron oxide particles and induced by the bulk magnetic susceptibility of SPIOs. The shift of the resonance frequency of iron labeled cells allowed us effectively suppress the host tissues with saturation RF pulse to improve MRI detection of grafted cells.

Conclusions: Iron oxide particles increase the resonance frequency of water proton signal. This shift permitted us to add the tissue/fat saturation RF pulse into the original SWIFT acquisition protocol and detect distinct hyperintense signals from grafted cells with minimal background signal from the host tissue.

[*]- Corresponding author: Sergey Magnitsky PhD, Director of Research Imaging Facility, Children's Hospital of Philadelphia, 3516 Civic Center Blvd, Abramson Bldg. Room 413, Philadelphia, PA 19104-4318, tel: 215 590 2222, magnitsksm@email.chop.edu.

Keywords

iron oxide; SWIFT; cell tracking; positive contrast; hypointense signal; susceptibility

Introduction.

A decrease in the number of Mesenchymal Stem Cells (MSCs) in bone marrow due to aging or any other reasons can lead to a reduction of osteogenesis and bone fracture [1–3]. An administration of MSCs has been shown to be a promising approach for the treatment of several bone degenerative disorders [4]. Several successful examples of MSC treatment of osteoporosis, osteoarthritis and bone fractures have been published recently [5–7]. In all these studies, the fate of the grafted cells was determined post mortem by histological staining. Translation of these new and promising therapeutic approaches into the clinic would be greatly facilitated by the development of non-invasive methods for tracking grafted MCSs in animals and patients.

MR imaging has several advantages for tracking of grafted cells compared to other imaging modalities [8]. This detection method produces tomographic images of grafted cells with a high spatial resolution. MRI does not employ ionizing radiation; thus, there are no exposure limitations on the number of studies that can be performed on a given subject. To distinguish donor cells from the host tissue, several contrast agents were implemented [9]. Iron oxide particles were recognized as the most potent MRI contrast agent for cellular imaging, and numerous preclinical and several clinical studies have been reported [8, 10–12]. The main disadvantage of the iron oxide particles as an MRI contrast agent is a hypointense signal intensity produced by this reagent on conventional T2*-weighted images. Determining the quantity of grafted cells is critically important for the therapeutic efficacy evaluation, but unfortunately, the “negative” contrast afforded by T2*-weighted imaging cannot be used for quantitative analysis in most cases. Also, the hypointense signal is difficult to detect in areas with a low signal intensity such as bone.

Several methods have been developed to recover MR signal from fast relaxing spins, which can be implemented for tracking of iron-labeled cells including Ultrashort Echo Time (UTE) [13–16], Zero Echo Time -ZTE [17–20], ZTE combined with Single Point Imaging (SPI) [21], and SWeep Imaging with Fourier Transformation (SWIFT) [22, 23]. Our group implemented the SWIFT sequence for detecting iron labeled cells. We have shown that SWIFT produces a hyperintense signal from solutions of iron oxide particles, while traditional sequences (spin and gradient echo) produce hypointense signals [24–28]. We were also able to quantify the amount of iron labeled cells in the tissue [29]. We performed *in vivo* experiments with cells labeled with 200 μg/mL = 3.56 mM of Fe because this concentration of the contrast agent provided us with a sharp hyperintense signal. However, similar to the conventional T2-weighted imaging, we observed a hypointense signal when we injected a concentrated suspension of iron labeled cells or high concentration of iron oxide particles.

The goal of this study was to delineate a reason for the hypointense signal in the tissue from concentrated solutions of iron labeled cells during SWIFT acquisition. We hypothesized that

the hypointense signal from high concentrations of iron oxide is due to 1) broadening of NMR line-width and 2) an alteration of the resonance frequency of water molecules around iron oxide centers. Besides, we were interested to optimize the SWIFT acquisition protocol to generate a robust hyperintense signal from high concentrations of grafted cells in a knee joint.

Methods

Iron oxide particles:

The FDA approved superparamagnetic iron oxide particles (SPIO) (Feraheme, Amag, Waltham, MA, USA) were used throughout this study.

MRI Phantom:

A phantom consisting of eight 200 μL mini-Eppendorf tubes with different Feraheme concentrations was created to determine the concentration range that yields an image with hypointense signal intensity with the SWIFT acquisition protocol. The Feraheme stock solution (537 mM = 30,000 μg/mL) was diluted with phosphate buffered saline (PBS) to produce 0; 0.89; 1.79; 3.57; 5.37; 10.74; 21.48; 357 mM (0; 50; 100; 200; 300; 600; 1,200 and 30,000 μg/mL) iron concentrations which were then transferred to the mini-Eppendorf tubes.

To detect and measure an effect of Feraheme on the resonance frequency of water protons different dilutions were tested. Techniques similar to those described above were used to generate iron oxide particle solutions of 0; 0.89; 3.56; 8.9; 17.9 mM (0; 50; 200; 500; 1000 μg/mL) which were transferred to standard 5 mm cylindrical or spherical-shape NMR bulb. The experiments were performed with NMR tubes oriented parallel or perpendicular to the main magnetic field. No susceptibility matching liquids were used. The spherical-shape of the NMR bulb minimizes bulk magnetic susceptibility effects and was used to estimate the proton resonance frequency shifts due to bulk magnetic susceptibility and chemical shift of water protons. The iron oxide solutions occupied only a spherical part of the bulb while the neck was filled with air.

Cells:

Mouse Mesenchymal Stem Cells (MSCs) for this study were kindly donated by Dr. N. E. Lane (Center for Musculoskeletal Health, the University of California at Davis School of Medicine, Sacramento, CA, USA). Cells were maintained on uncoated T-75 plastic flasks and split at a ratio of 1:10, once a week by gentle trypsinization and 700 rpm centrifugation for 2 min. Minimum Essential Medium α (MEM α) with 10% fetal bovine serum (FBS) and 1% Antibiotic-Antimycotic (PSA) supplements were used as growth media.

Labeling of cells with iron oxide particles:

To label MSCs, the 3.57 mM of Feraheme solution was mixed with 1.5 μg of poly-L-lysine (PLL, Sigma, St. Louis, MO, USA) and stirred at room temperature for 60 min [10, 29–31]. The Feraheme-PLL mixture was then added into flasks of adherent cells and incubated overnight. Labeled cells were washed three times with PBS and harvested by gentle

trypsinization and centrifugation. This labeling technique was used in our previous experiments and led to the uniform labeling of MSCs with an average concentration of ~20 pg of iron per cell. This combination of the transfection and contrast agents was found not toxic for MSCs, based on a proliferation and differentiating assays. More information about labeling procedure can be found in our earlier publication [29].

In vivo Implantation of MSCs:

All procedures were conducted in accordance with the National Institute of Health Guide for the Care and Use of Laboratory Animals and were approved by the Institutional Animal Care and Use Committee of the University of California at San Francisco and the University of Minnesota. 4×10^6 of MSCs labeled with 3.57 mM of iron oxide were re-suspended in PBS with the final volume of 50 μL and injected into knee joints of hind limbs of adult female rats (n=10). During imaging experiments, animals were anesthetized with a mixture of 2% isoflurane and pure oxygen that was delivered via a nose cone at a rate of 0.6 liters per hour. MR imaging was performed before and 30–60 min after injection of labeled cells. In another experiment (n=3) 20 μL of 20 $\times10^6$ of MSCs labeled with the same concentration of the iron oxide was injected into a muscle tissue of rat's hind limb.

NMR line-width measurement:

NMR spectra of different concentrations of the iron oxide solutions were recorded using a 400 MHz high-resolution NMR scanner (Agilent, Santa Clara, CA) with the following parameters: spectrum bandwidth 400 kHz, number of point 32K, acquisition time = 3 sec, repetition time (TR) = 10 sec, number of excitations (NEX) = 2. Measurements of the resonance frequency of different iron oxide solutions were performed with a 5-mm high-resolution NMR probe

MR imaging:

Imaging experiments were performed with a horizontal bore 7 T or 9.4 T magnet interfaced to an Agilent console (Agilent, Santa Clara, CA). Images of the phantom with eight different concentrations of the iron oxide solutions were acquired with a 38 mm ID Agilent quadrature birdcage coil. The *in vivo* studies were acquired using a 9.4 T magnet with a homemade 20 mm transmit-receive 2-loop surface coil. To increase B1 field homogeneity the animal's knees were placed between loops. The position of the animals' knee was determined with a gradient echo sequence using the following parameters: TR=10 msec, echo time (TE) = 4 msec, excitation flip angle = 15°, the field of view (FOV) = 4 or 3 cm, matrix size = 128×128, slice thickness = 1 mm, NEX = 2. To minimize the effect of the spatially dependent B1-field produced by the surface coil, we positioned the coil with the same distance from the injection site. A permanent marker was used to spot the injection site. In addition, after positioning of the coil, we performed slice selective calibration of the 90° pulse. The slice with the hypointense signal from the grafted cells was selected based on gradient echo scout images.

SWIFT imaging:

The imaging experiment with eight different solutions of iron oxide particles was performed at 7 T using the following parameters: RF excitation was performed with an amplitude- and frequency-modulated pulse of the hyperbolic secant (HS*n*) family pulses [32] with stretching factor (*n*) of 2 and a time-bandwidth product of 64. The pulse was oversampled by a factor of 16 [32]. Data were collected in 64 gaps in the HS*n* pulse, and after the pulse, 192 sample points were acquired without gaps. Other parameters were: bandwidth = 100 kHz; readout time = 2.6 ms, excitation flip angle varied from 1 to 26°; number of views = 8192, evenly distributed over the surface of a sphere in k-space; NEX = 1; FOV = 40 × 40 × 40 mm^3, and total scan time ~3 minutes.

In vivo detection of grafted cells was performed using a 9.4T magnet with the following parameters: Radial 3D MB-SWIFT images [23] were acquired with 4 phase shifted hard pulses of 5.2 μs length (with 2.6 μs dead time), TR = 1.9 ms, excitation/acquisition bandwidths 192/384 kHz, number of views = 96000. To saturate the host tissue, we utilized a magnetization preparation scheme by applying double-banded Gaussian RF-pulse [33]. The saturation 90-degree pulse with ~200 Hz bandwidth was tuned to the water (4.7 ppm) and fat (1.3 ppm) frequencies and applied sequentially after an acquisition of every 16's projections. Water and fat saturation pulses were created separately using standard Agilent software for RF-pulse design and fused together to achieve double saturation. Proton signal from host tissue in our experiments was usually around 150–200 Hz; therefore, we decided to use the same bandwidth for the saturation pulse.

Histology:

Five days after *in vivo* experiments, rats were sacrificed under deep anesthesia. Legs were removed and frozen at 77K. To perform histological staining muscle tissues were removed and specimens were immersed into 10% neutral buffered formalin and decalcified with EDTA. After the decalcification tissues were embedded in paraffin and five μm-thick sections were stained with Prussian Blue.

Prussian Blue staining for detection of iron:

Slides were placed in a Coplin jar containing a 2:1 mixture of 2% potassium ferrocyanide and 2% hydrochloric acid for 30 minutes in a 37°C water bath. The slides were then rinsed with distilled water and counterstained with nuclear fast red (Vector Laboratories) for 20 minutes.

Results

Figure 1 shows SWIFT images of the phantom with different concentrations of iron oxide solutions acquired with 4° and 24° excitation flip angles. The windowing level of both images is the same. Tubes with low concentrations (0; 0.89; 1.79; 3.57 mM) of the iron oxide were visible on SWIFT images acquired with the low flip angle, while the high concentrations of the iron oxide (5.37; 10.74; 21.48 mM) were detected on the high flip angle images. Images of tubes with high concentrations of iron oxide (5.37; 10.74; 21.48 mM) revealed significant blurring. No signal from the highest concentration of the iron

oxide particles (537 mM) was detected even at the highest possible flip angle and any windowing level. We hypothesized that blurring of the images was a result of two effects: 1) broadening of the NMR line due to shortening of T2, and 2) off-resonance acquisition of the MR signal. To test this hypothesis, we conducted the measurements described below.

Table 1 depicts the NMR linewidth of different concentrations of the iron oxide solutions. As expected, significant broadening was detected in the concentrated iron oxide solutions. At the highest concentration of iron oxide measured (537 mM), the line width was more than 14 kHz (Table 1), and we were not able to generate an image of vial with this concentration (Figure 1). The solutions of 10.74 and 21.48 mM of iron oxide had a linewidth of more than 300 and 600 Hz respectively and exhibited blurry images (Figure 1B).

We also measured the resonance frequency of different concentrations of the iron oxide particles. We detected an increase of the resonance frequency of proton signal in response to the increase of the iron oxide concentration. Figure 2 (blue line) shows the linear dependence ($y=0.277x$) of the frequency shift on the concentration of the iron oxide particles when the main magnetic field was parallel to the long axis of a cylindrical NMR tube. When the main magnetic field was 90^o to the long axis of the NMR tube the slope of the line was twice less ($y=0.149x$) (Figure 2 orange line). Much weaker ($y=0.029\ x$) dependence of the frequency shift on the concentration of the iron oxide was detected in the spherical bulb (Figure 2 grey line).

The discovery of the proton frequency shift led us to an idea to saturate the water signal from the host tissue and detecting the signal from iron labeled donor cells only. Figure 3A shows the anatomical SWIFT image of a rat knee before the injection, while Figure 3B shows the SWIFT image of the same knee, but with the saturation achieved by the dual frequency-selective Gaussian-shaped RF pulse tuned to the water (4.7 ppm) and fat (1.3 ppm) signals. The pulse successfully suppressed MR signals from muscle tissues while the fat was suppressed less efficient probably due to broader NMR line. Figure 3C shows the tissue/fat saturated image of the same knee after administration of 4×10^6 iron labeled MSCs in the total volume of 50 μL. A distinct hyperintense signal from the graft was detected in this experiment.

To confirm *in vivo* detection of iron oxide particles in the tissue we performed a histological analysis. After *in vivo* experiment, the animals were sacrificed and the presence of iron was validated by staining. Figure 3D presents the Prussian blue staining of the knee joint. Blue color on the cartilage tissue indicated the presence of iron in the tissue.

To confirm our hypothesis that the proposed method can be used to convert a hypointense signal from a high concentration of grafted cells into a hyperintense signal, we injected a 20 μL suspension of 20×10^6 iron-labeled MSCs into a rat muscle tissue. The negative contrast was detected in the regular SWIFT image (Figure 4B). After the implementation of the tissue/fat saturation RF pulse, the hyperintense signal was discovered (Figure 4C).

Discussion

Generation of a hyperintense MRI signal from iron labeled cells is essential for the quantification of grafted cells and the evaluation of stem cell therapy efficacy. The SWIFT sequence produces a positive contrast from diluted iron-labeled cells. However, when the concentration of grafted cells becomes high, the hypointense contrast was observed. In this study, we have shown that the negative contrast from a high concentration of grafted cells is a result of 1) broadening of the NMR line and 2) a shift of the water proton frequency in the vicinity of the iron oxide centers. This frequency shift is linearly proportional to the concentration of the iron oxide. We propose to use this frequency shift in the tissue saturation scheme to generate the hyperintense MRI signal from diluted and concentrated solutions of grafted cells with minimum background signal from the host tissue.er

Traditionally iron labeled cells in the tissue have been detected with T2/T2*-weighted MR imaging. Short T2/T2* values of water molecules around the iron oxide particles manifest as signal voids on conventional MR images. Because there is no reliable method to quantify a signal void and the detection is challenging especially in bone tissues, we investigated the capability of SWIFT MRI to overcome these limitations. This ultra-short-echo time technique allowed us to eliminate T2 dependence and produces T1-weighted images of grafted cells. However, the positive signal intensity was not always observable in our cell transplantation experiments. The injection of very concentrated solutions of the labeled cells or a very high concentration of the iron oxide particles produced the hypointense signal on SWIFT images. An implementation of MB-SWIFT sequence [23] with extremely high bandwidths also yielded hypointense signal. We were interested to understand these signal variations and to improve our imaging protocol to generate consistent imaging data.

We tested the ability of the SWIFT sequence to recover an NMR signal from a very concentrated solution of iron oxide. In our experiments on the phantom containing different concentrations of the iron oxide, we detected images of all iron solutions (concentrations 0–21.48 mM) except the tube with 537 mM of the iron oxide (Figure 1). The NMR line-width of the proton signal of the 537 mM of iron oxide solution was about 14 kHz, which translates to T2 ~ 22 μsec. The echo-time in our SWIFT experiment was about 2 μsec. That means our acquisition protocol has a capacity to detect the signal from this solution, and there must be another reason preventing a visualization of the tube. We also noticed that images of the tubes with less concentrated iron oxide solutions (10.74 and 21.48 mM) were blurry. The line width of the NMR signal of 10.74 mM was around ~ 340 Hz, while the acquisition bandwidth per pixel was ~390 Hz. Since the NMR linewidth and bandwidth per pixel were comparable for 10.74 mM concentration, it was unclear why the image was so blurry. Image blurring at high iron oxide concentrations was also reported earlier by Zhang [24]. We hypothesized that the loss of the image sharpness could be a result of an off-resonance acquisition.

Recording of NMR spectrum of different concentrations of the iron oxide particles revealed the increase of the proton resonance frequency in a linear manner (Figure 2). It is well known that the paramagnetic particles can cause a shift of the resonance frequency of a nuclear spin by two additive mechanisms: the hyperfine shift (chemical shift) and the bulk

magnetic susceptibility shift (an alteration of main magnetic field) [34]. To separate these two effects, we performed experiments on iron-oxide samples in containers of different shapes. In the experiments conducted with the cylindrical NMR tube, we detected the resonance frequency change induced by both hyperfine and bulk magnetic susceptibility shifts. The spherical bulb was used to estimate only the hyperfine shift of the water protons in the iron oxide solutions [34]. The slope of the frequency shift of the spherical phantom was ten-fold less than the slope of the cylindrical samples (0.28 vs. 0.029 slopes of blue and gray lines in Figure 2). This result indicated that the bulk magnetic susceptibility changes of the main magnetic field were ten times greater than the hyperfine shift (chemical shift) and reached ~3.75 ppm (~1500 Hz) at the iron concentration of 17.9 mM (1000μg/mL). We also observed a strong orientation dependence of the resonance frequency shift and the main magnetic field. The slope of cylindrical tube oriented parallel to the main magnetic field was twice bigger than the slope of the tube oriented perpendicular to the B0 field (0.28 vs 0.15 for the parallel and perpendicular orientation), which was consistent with theoretical predictions and previous reports [35–37].

The slope of the blue line in Figure 2 proportional to the magnets susceptibility and can be used to measure this quality of iron oxide particles. Because the magnetic susceptibility of a solution is a weighted sum of the magnetic susceptibilities of an individual component, this method of measurements of magnetic susceptibility will be useful for the chemists who are developing magnetic nanoparticles and has access to the exact composition of the experimental solution. In this study, we have presented measurements conducted on Feraheme only. In preliminary experiments with mesoporous-silica-coated iron oxide particles, the frequency shifts were larger than those of Feraheme (data not shown). These results indicated that proper characterization of the frequency shift would be necessary for experiments with different types of iron oxide particles.

An injection of iron labeled cells directly into a knee joint was recognized as an effective method to supply therapeutic cells for the treatment of osteoporosis or osteoarthritis. This technique allows delivery of a much larger number of the cells into the injured area as compared to an intravenous administration. Our group is developing MRI methods for *in vivo* monitoring of grafted cells after injection into a knee joint. To better visualize grafted cells we implemented tissue saturation scheme. In our *in vivo* experiments, water proton signal from rat knee had ~150 – 200 Hz linewidth; therefore, we decided to use the same bandwidth for the tissue saturation pulse. Implementation of ~200 Hz-bandwidth RF pulse led to the effective suppression of tissues signal (Fig.3B), at the same time the signal from grafted cells was detected (Fig.3C). We incubated MSCs with 3.57mM of iron oxide. In an aqueous solution, this concentration of the iron oxide can induce frequency shift which has a range from 39 Hz for a spherical distribution of the particles to 388 Hz for a cylindrical configuration with a parallel orientation to the main magnetic field. The application of 150, 200 and 250 Hz-bandwidth saturation pulses (data not shown) on host tissue did not revile significant changes in the signal intensity from grafted cells. We believed, the little effect of tissue saturation pulse on the signal from grafted cells can be attributed mainly to the fast recovery (T1(Fe=3.57mM) < 200 ms) of the cells' signal compare to a significantly longer revival of the signal from host tissue (T1(muscle) >1000 ms). In addition, these results suggest that the orientation of the iron oxide particles in the tissue is not spherical and most

likely cylindrical with the long axis parallel to the main magnetic field. It is also apparent that the frequency shift plays a more important role in a production of the hypointense signal from concentrated solutions of the grafted cells in the tissue then broadening of NMR signal. More investigation requires to understand the orientation of particles in the tissue fully. Tight compartmentalization of iron oxide particles inside of the cells, slow water exchange between intra- and extracellular space, a restricted diffusion of the iron particles and water molecules inside of donor cells, the high viscosity of intracellular space can produce additional alterations of the resonance frequency and T1 of water molecules inside of labeled cells. Another step to enhance the detection of grafted cells is an acquisition of MR images with different frequency offsets. Noll et al [38] suggested a reconstruction method of images acquired with a frequency offset. This method was successfully implemented for a reduction of blurring of SWIFT images of phantoms with different concentrations of iron oxide particles [24].

We believe, that alteration of the resonance frequency due to the iron oxide particles is a universal effect and does not accrue exclusively during SWIFT acquisition. Thus, the tissue saturation technique can be implemented for the detection of grafted cells with other acquisition protocols such as UTE and ZTE.

In our study, we have shown that administration of a concentrated suspension of iron labeled cells can be detected with MRI imaging and a hyperintense contrast from grafted cells is achievable with the proposed technique. The number of cells which can be injected into a human patient varies and depends on the type of therapy[39]. Immunotherapy treatment required billions of therapeutic cells. A few clinical trials with implantation of iron-labeled stem cells were performed so far. The range of implanted cells in these studies was from 300,000 of iron labeled islet to 10^8 dendritic cells. In this study, we demonstrated the detection of high concentrations of iron labeled cells with hyperintense contrast. A determination of the lowest level of grafted cell that can be detected with the proposed method is essential for the clinical translation. In our previous work [40], we proposed a protocol to determine the sensitivity of T2-weighted sequences for the detection of the iron oxide particles. We are adopting this technique for the SWIFT acquisition protocol and will report the results in a separate publication.

Conclusion

Iron oxide particles not only broaden NMR linewidth but also increase the resonance frequency of surrounding water protons. This frequency shift is linearly proportional to the concentration of the iron oxide particles and primarily arise from bulk magnetic susceptibility. The difference in the resonance frequencies of host water protons and the iron labeled donor cells can be used for the detection of grafted cells: an application of a tissue saturating RF pulse allows to detect distinct hyperintense signal from grafted cells with a minimal signal from host tissue.

Acknowledgment

Research reported in this publication was supported by the National Institute of Arthritis and Musculoskeletal and Skin Diseases of the National Institutes of Health under Award R21 AR068507 (SM) and P41 EB015894 (MG).

The content is solely the responsibility of the authors and does not necessarily represent the official views of the National Institutes of Health. We want to thank Professor Felix Wehrli (University of Pennsylvania) and Professor Charles Springer (Oregon Health & Science University Hospital) for the useful discussion. We also would like to thank Tony Huynh for the help with MRI acquisition and animal preparations.

References

1. Stolzing A, et al., Age-related changes in human bone marrow-derived mesenchymal stem cells: consequences for cell therapies. Mech Ageing Dev, 2008 129(3): p. 163–73. [PubMed: 18241911]
2. Katsara O, et al., Effects of donor age, gender, and in vitro cellular aging on the phenotypic, functional, and molecular characteristics of mouse bone marrow-derived mesenchymal stem cells. Stem Cells Dev, 2011 20(9): p. 1549–61. [PubMed: 21204633]
3. Bonyadi M, et al., Mesenchymal progenitor self-renewal deficiency leads to age-dependent osteoporosis in Sca-1/Ly-6A null mice. Proc Natl Acad Sci U S A, 2003 100(10): p. 5840–5. [PubMed: 12732718]
4. Pittenger MF, et al., Multilineage potential of adult human mesenchymal stem cells. Science, 1999 284(5411): p. 143–7. [PubMed: 10102814]
5. Watson L, Elliman SJ, and Coleman CM, From isolation to implantation: a concise review of mesenchymal stem cell therapy in bone fracture repair. Stem Cell Res Ther, 2014 5(2): p. 51. [PubMed: 25099622]
6. Bornes TD, Adesida AB, and Jomha NM, Mesenchymal stem cells in the treatment of traumatic articular cartilage defects: a comprehensive review. Arthritis Res Ther, 2014 16(5): p. 432. [PubMed: 25606595]
7. Yao W and Lane NE, Targeted delivery of mesenchymal stem cells to the bone. Bone, 2015 70: p. 62–5. [PubMed: 25173607]
8. Naumova AV, et al., Clinical imaging in regenerative medicine. Nat Biotechnol, 2014 32(8): p. 804–18. [PubMed: 25093889]
9. Srivastava AK, et al., Advances in using MRI probes and sensors for in vivo cell tracking as applied to regenerative medicine. Dis Model Mech, 2015 8(4): p. 323–36. [PubMed: 26035841]
10. Bulte JW, et al., Preparation of magnetically labeled cells for cell tracking by magnetic resonance imaging. Methods Enzymol, 2004 386: p. 275–99. [PubMed: 15120257]
11. Bulte JW, et al., Monitoring stem cell therapy in vivo using magnetodendrimers as a new class of cellular MR contrast agents. Academic Radiology, 2002 9(Suppl 2): p. S332–5. [PubMed: 12188266]
12. Bulte JW, Duncan ID, and Frank JA, In vivo magnetic resonance tracking of magnetically labeled cells after transplantation. Journal of Cerebral Blood Flow & Metabolism, 2002 22(8): p. 899–907. [PubMed: 12172375]
13. Bergin CJ, Glover GH, and Pauly JM, Lung parenchyma: magnetic susceptibility in MR imaging. Radiology, 1991 180(3): p. 845–8. [PubMed: 1871305]
14. Gatehouse PD and Bydder GM, Magnetic resonance imaging of short T2 components in tissue. Clin Radiol, 2003 58(1): p. 1–19. [PubMed: 12565203]
15. Boujraf S, et al., Ultrafast bold fMRI using single-shot spin-echo echo planar imaging. J Med Phys, 2009 34(1): p. 37–42. [PubMed: 20126564]
16. Bracher AK, et al., Feasibility of ultra-short echo time (UTE) magnetic resonance imaging for identification of carious lesions. Magn Reson Med, 2011 66(2): p. 538–45. [PubMed: 21360742]
17. Hafner S, Fast imaging in liquids and solids with the Back-projection Low Angle ShoT (BLAST) technique. Magn Reson Imaging, 1994 12(7): p. 1047–51. [PubMed: 7997092]
18. Madio DP and Lowe IJ, Ultra-fast imaging using low flip angles and FIDs. Magn Reson Med, 1995 34(4): p. 525–9. [PubMed: 8524019]
19. Weiger M, Pruessmann KP, and Hennel F, MRI with zero echo time: hard versus sweep pulse excitation. Magn Reson Med, 2011 66(2): p. 379–89. [PubMed: 21381099]
20. Weiger M, et al., High-resolution ZTE imaging of human teeth. NMR Biomed, 2012 25(10): p. 1144–51. [PubMed: 22290744]

21. Grodzki DM, Jakob PM, and Heismann B, Ultrashort echo time imaging using pointwise encoding time reduction with radial acquisition (PETRA). Magn Reson Med, 2012 67(2): p. 510–8. [PubMed: 21721039]
22. Idiyatullin D, et al., Fast and quiet MRI using a swept radiofrequency. J Magn Reson, 2006 181(2): p. 342–9. [PubMed: 16782371]
23. Idiyatullin D, Corum CA, and Garwood M, Multi-Band-SWIFT. J Magn Reson, 2015 251: p. 19–25. [PubMed: 25557859]
24. Zhang J, et al., Quantifying iron-oxide nanoparticles at high concentration based on longitudinal relaxation using a three-dimensional SWIFT Look-Locker sequence. Magn Reson Med, 2014 71(6): p. 1982–8. [PubMed: 24664527]
25. Zhang J, et al., Gradient-modulated SWIFT. Magn Reson Med, 2016 75(2): p. 537–46. [PubMed: 25800547]
26. Zhang J, et al., Capturing fast relaxing spins with SWIFT adiabatic rotating frame spin-lattice relaxation (T1rho) mapping. NMR Biomed, 2016 29(4): p. 420–30. [PubMed: 26811973]
27. Zhang J, et al., Quantification and biodistribution of iron oxide nanoparticles in the primary clearance organs of mice using T1 contrast for heating. Magn Reson Med, 2016.
28. Zhou R, et al., SWIFT detection of SPIO-labeled stem cells grafted in the myocardium. Magn Reson Med, 2010 63(5): p. 1154–61. [PubMed: 20432286]
29. Magnitsky S, et al., Positive contrast from cells labeled with iron oxide nanoparticles: Quantitation of imaging data. Magn Reson Med, 2017 78(5): p. 1900–1910. [PubMed: 28097749]
30. Frank JA, et al., Magnetic intracellular labeling of mammalian cells by combining (FDA-approved) superparamagnetic iron oxide MR contrast agents and commonly used transfection agents. Academic Radiology, 2002 9(Suppl 2): p. S484–7. [PubMed: 12188316]
31. Frank JA, et al., Clinically applicable labeling of mammalian and stem cells by combining superparamagnetic iron oxides and transfection agents. Radiology, 2003 228(2): p. 480–7. [PubMed: 12819345]
32. Idiyatullin D, et al., Gapped pulses for frequency-swept MRI. J Magn Reson, 2008 193(2): p. 267–73. [PubMed: 18554969]
33. Garwood M, et al., ‘Capturing Signals from Fast-relaxing Spins with Frequency-Swept MRI: SWIFT. eMagRae, 2012.
34. McConnell HM and Robertson RE, Isotropic Nuclear Resonance Shifts. THE JOURNAL OF CHEMICAL PHYSICS, 1958 29(6): p. 1361–1365.
35. Albert MS, et al., Aqueous shift reagents for high-resolution cation NMR. VI. Titration curves for in vivo 23Na and 1H2O MRS obtained from rat blood. NMR Biomed, 1993 6(1): p. 7–20. [PubMed: 8457429]
36. Albert MS, et al., Susceptibility changes following bolus injections. Magn Reson Med, 1993 29(5): p. 700–8. [PubMed: 8505909]
37. Chu SC, et al., Bulk magnetic susceptibility shifts in NMR studies of compartmentalized samples: use of paramagnetic reagents. Magn Reson Med, 1990 13(2): p. 239–62. [PubMed: 2156125]
38. Noll DC, et al., Deblurring for non-2D Fourier transform magnetic resonance imaging. Magn Reson Med, 1992 25(2): p. 319–33. [PubMed: 1614315]
39. Bulte JW, In vivo MRI cell tracking: clinical studies. AJR Am J Roentgenol, 2009 193(2): p. 314–25. [PubMed: 19620426]
40. Magnitsky S, et al., In vivo and ex vivo MR imaging of slowly cycling melanoma cells. Magn Reson Med, 2011 66(5): p. 1362–73. [PubMed: 21523820]

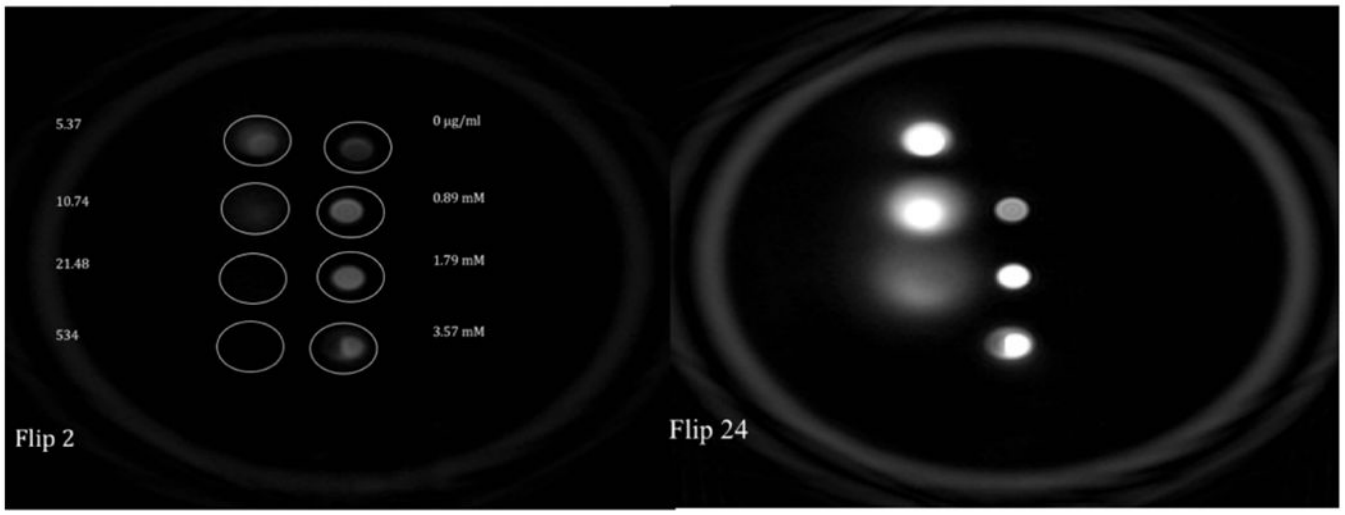

Figure 1.
SWIFT MR image of the phantom with different concentrations of iron oxide solutions acquired with (A) 4° (B) 24° excitation flip angles.

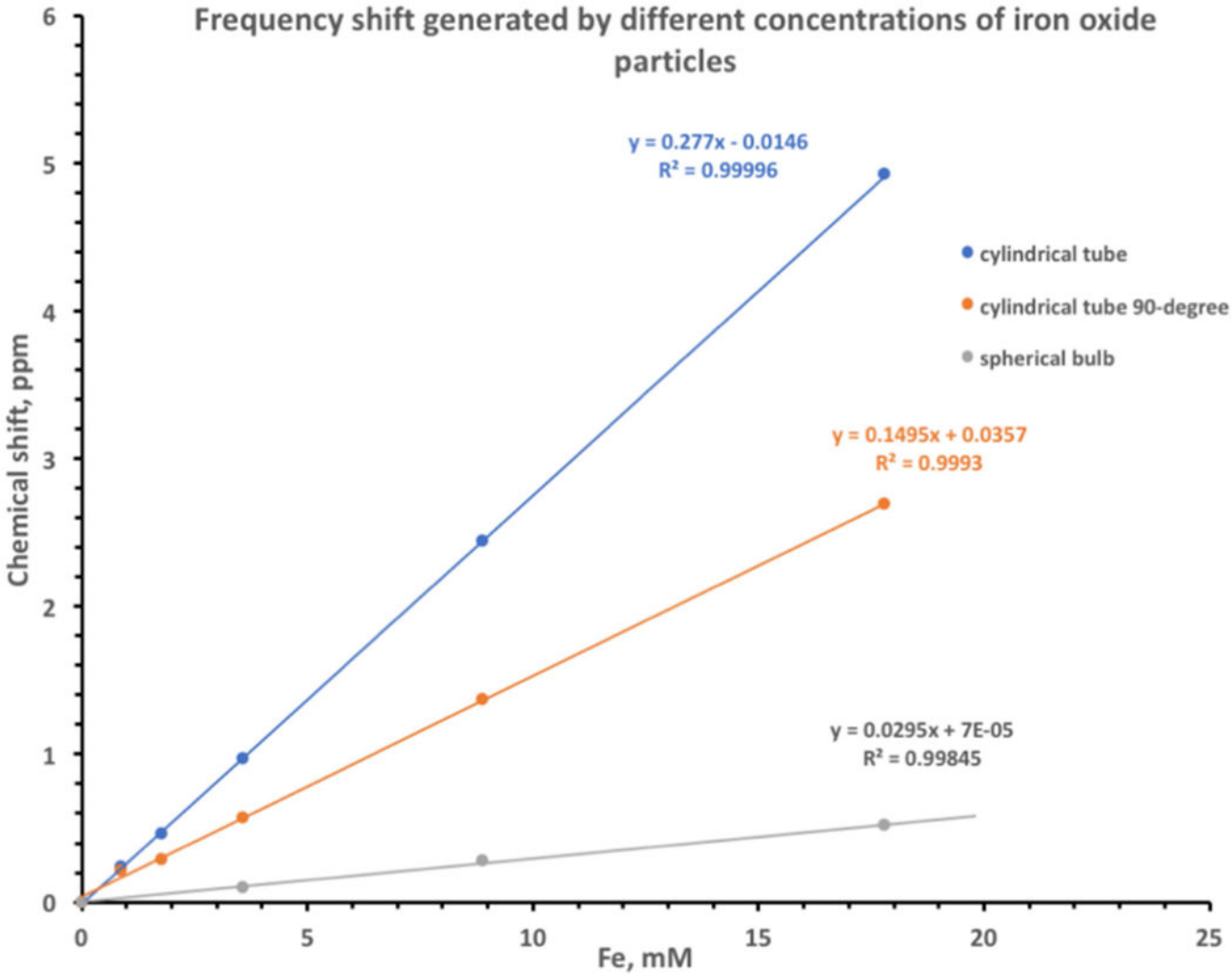

Figure 2.

Frequency shift generated by different concentrations of iron oxide particles. Blue – iron oxide solution in a cylindrical NMR tube oriented parallel to the main magnetic field. Orange – iron oxide solution in a cylindrical NMR tube oriented perpendicular to the main magnetic field, Gray – iron oxide solution in a spherical NMR bulb.

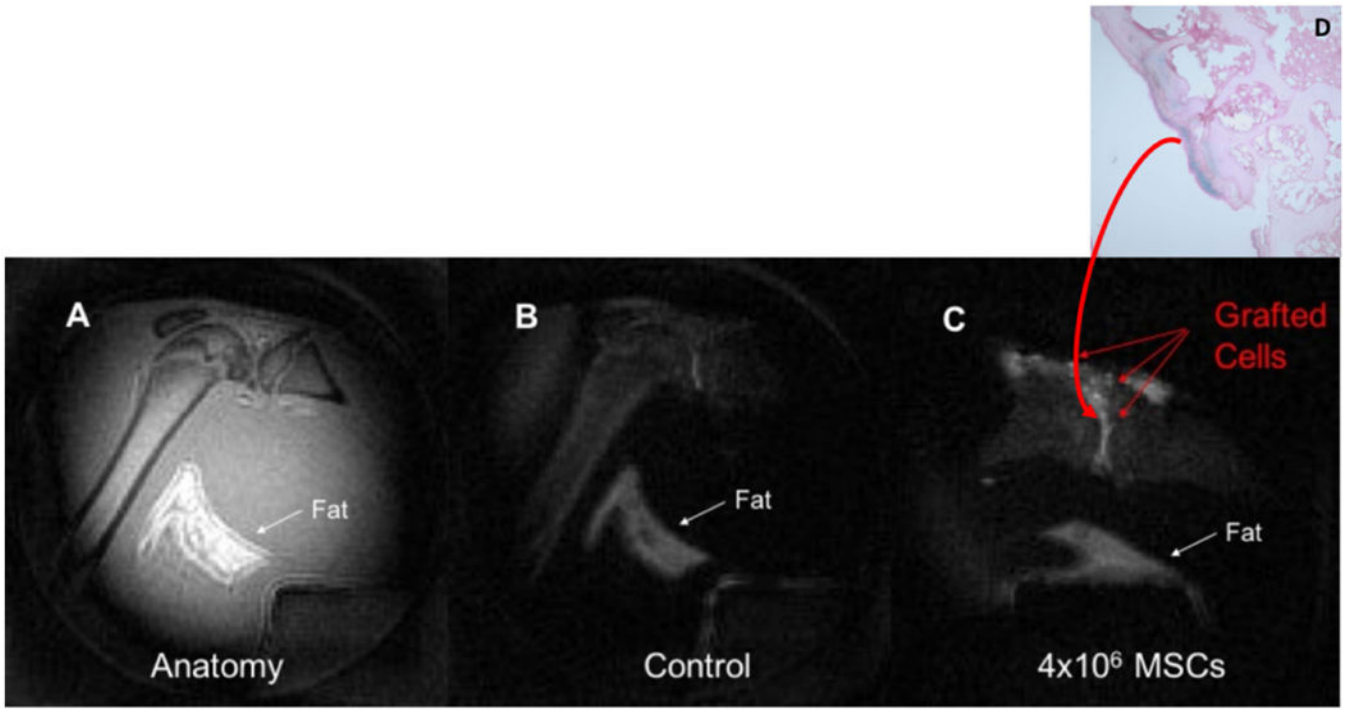

Figure 3.

(A) – Anatomical SWIFT MR image of a rat knee, (B) – SWIFT MR image of the same knee after application of tissue saturation pulse, (C) – tissue saturated SWIFT image of the same knee after administration of iron labeled MSCs, (D) – Prussian blue staining of the knee tissue. Blue area in the cartridge tissue indicates the presence of iron in the tissue.

Figure 4.
(A) –SWIFT MR image of a rat knee, (B) - SWIFT MR image of a rat knee after administration of the high concentration of iron labeled MSCs into a muscle tissue. The hypointense signal from grafted cells was detected, (C) – the same image as (B) with tissue saturation pulse. Hyperintense signal from grafted cells was recovered.

Table 1.

Line widths of the NMR proton signal from different concentrations of the iron oxide particles.

Fe concentration (mM)	Fe concentration (μg/mL)	NMR line width (Hz)
0.89	50	69.5 ± 11.3
1.79	100	101.1 ± 19.5
3.57	200	161.9 ± 28.6
8.9	500	340.8 ± 63.3
17.9	1000	640.5 ± 117.8
537	30,000	~14000 ± 2000